Received: 19 March 2022 | Revised: 17 May 2022 | Accepted: 30 May 2022

DOI: 10.1002/app.52755

RESEARCH ARTICLE

Journal of Applied Polymer Science WILEY

Multifunctional and stretchable graphene/textile composite sensor for human motion monitoring

Yi Zhou | **Connor Myant** | **Rebecca Stewart**

Dyson School of Design Engineering, Imperial College London, London

Correspondence
Yi Zhou, Dyson School of Design Engineering, Imperial College London, London SW7 2DB.
Email: y.zhou20@imperial.ac.uk

Abstract

Sensors based on electronic textiles (e-textiles) have become increasingly prominent in the field of biomechanical monitoring technology due to multiple properties such as being lightweight, flexible, and comfortable, with increasing potential in incorporating into long-term monitoring devices. Previous research has been conducted into textile strain sensors based on graphene for human motion monitoring, however most graphene e-textile strain sensors exhibit poor sensitivity and stretchability. To our knowledge, no previous research has looked at knitted graphene-based fabrics in regards to the fabric composition of the substrate. In this paper, we propose a graphene/fabric composite sensor using a cost-effective dip coating method of an acrylic/Spandex knit fabric, and further explores its mechanical, electrical, and sensing properties. The developed graphene/textile composite sensor has a wide sensing range (up to 344%) and exhibits a good sensitivity with a high gauge factor of up to 16. As a wearable sensor, our sensing fabric can detect both large and subtle human motions and is able to distinguish between various ranges of joint movements, demonstrating its ability to function as a human motion monitoring system. Our sensor further exhibits the ability to be used as a supercapacitor or capacitive pressure sensor.

KEYWORDS

composites, fullerenes, graphene, nanotubes, sensors and actuators, textiles

1 | INTRODUCTION

Recently, electronic textiles (e-textiles) have been widely applied in fields of energy storage systems,[1–3] human-machine interfaces,[4,5] sports[6] and personalized health monitoring systems,[7–9] and have attracted extensive attention in both industrial and academic fields. E-textiles are suitable as flexible sensors owing to their unique flexibility, wearability, stretchability, and facile interaction with human skin.[9,10] Flexible e-textile sensors can be applied in different wearable devices to monitor and collect various physiological data related to the human body, providing independent monitoring in real-time.[11,12]

The strain sensor is one of the most commonly used sensors because it can detect mechanical deformations or structural changes, and has great potential to be applied in wearable devices to monitor various human

movements.[13–17] It requires both great stretchability and high sensitivity to deal with high and small strains during human motion monitoring.[18] At present, commonly used composite strain sensors are usually made by addition of metal or inorganic semiconductor materials which have a more stable performance, but their inherent shortcomings include increased size and weight, poor stretchability and a limited sensing range which are undesirable for embedding into wearable sensor matrices.[19] This further limits their application in the fields of electronic skin interfaces, human physiological monitoring, human-machine interface and so forth.[20–23] Textiles are a more ideal substrate, with their large surface area, breathability and flexibility making them suitable for functionalizing materials over conventional strain sensor materials.[9,24] They can also be more cost effective and lightweight.[25–27]

Various carbon materials, conductive polymers and metals have been used to coat fabrics to fabricate sensors.[28–31] Among various conductive materials, graphene has outstanding electrical, mechanical, and thermal properties, which exhibits great potential as a conductive substrate in textile strain sensors.[32–35] Many functional textile sensors can be developed through chemical vapor deposition (CVD),[36] producing graphene oxide-based fabrics and reduced graphene oxide-based textiles.[37,38] However, graphene-based sensors fabricated by CVD are often expensive and difficult to control the size of generated graphene compounds.[39] Also, sensors using graphene oxide or reduced graphene oxide require strong acids during fabrication process, which requires a long production time and have poor electrical conductivity.[40]

In addition, most of the reported graphene-based textile strain sensors have poor stretchability and sensitivity when monitoring large-scale body movements. This is potentially because of the selection of fabric structure and yarn composition used as the substrate. The stretchability of the fabric is determined by both the material and fabric structure, but most of the fabric's stretch and recovery characteristics are decided by the elasticity of the underlying yarn.[18] For example, when comparing graphene-sensors with a single yarn or filament as the substrate, the sensing range and gauge factor can range from 46% and 0.94 with a nylon filament[41] to 50% and 0.1 with a flax yarn[42] to 100% and 0.5 with a silicone yarn.[43] When the yarn or filaments are arranged into a textile and then functionalized with graphene, how that textile is fabricated appears to affect the performance. A fabric consisting of wool yarn in a woven structure can produce a limited sensing range of 3% and gauge factor of 223[44] while a cotton yarn in knitted structure can have a much wider sensing range of 150% but with a gauge factor of 0.31.[45]

Although there have been numerous studies investigating graphene-based fabric sensors, few studies have investigated the role of textiles as a substrate in graphene-based sensors. In particular, previous research has not directly examined the effect of the yarn composition within a knitted textile stretch sensor substrate. Optimization of the textile design has the potential to produce strain sensors with high sensitivity and a broad sensing range.[18,46] In this study, graphene-based sensing fabrics are designed and knitted with yarns of differing materials and fabricated using a simple dip coating method. The sensor with the best initial performance is examined further looking at the microstructure, mechanical, electrical and sensing properties along with its capability in human motion monitoring. In addition, we explore the potential applications of our graphene-based fabrics as a supercapacitor and a capacitive pressure sensor.

2 | EXPERIMENTAL SECTION

2.1 | Materials

Five different yarns were selected for testing: fine cotton yarn (100% cotton); merino wool yarn (100% wool); lambswool yarn (100% lambswool); fine silk yarn (100% silk); and acrylic/Spandex yarns (90% acrylic and 10% Spandex). All were purchased from Tengxiao Yarn Ltd. (Yiwu, China). These five yarns were chosen because they are all commonly used natural and composite yarns which possess a desirable softness combined with flexibility.

Graphite intercalation compound (GIC) was provided by Huatai Tech Ltd. (Qingdao, China). Acetone was purchased from Aladdin Biochemical Technology Company (Shanghai, China).

2.2 | Fabrication of knitted sensing fabrics

Fabrics were knit with each of the selected yarns and then coated with graphene nanoplatelets (GNPs), as detailed in the following section.

2.2.1 | Fabrication of knitted fabrics

The different samples of knitted fabric were manufactured using the cotton, merino wool, lambswool, fine silk and acrylic/Spandex yarns. A gauge 10 Dubied double bed knitting machine (10 needles per inch) with a stitch tension of 9 was used to knit the fabrics. The gauge and

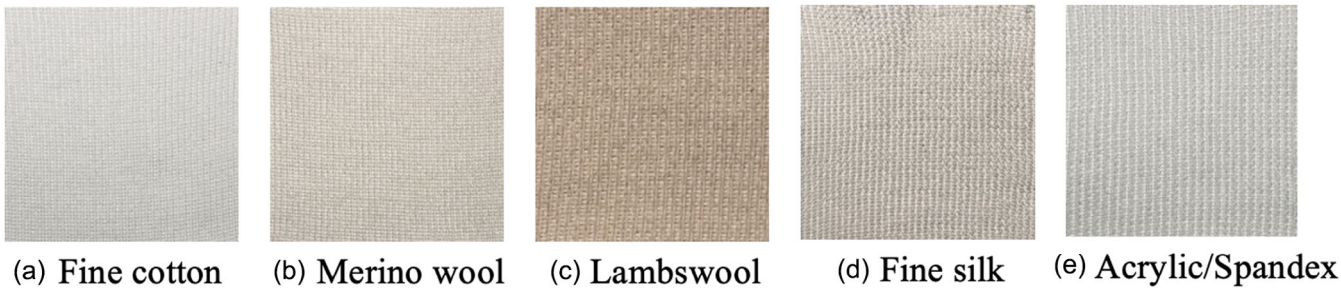

FIGURE 1 Photographs of the five knitted fabrics [Color figure can be viewed at wileyonlinelibrary.com]

FIGURE 2 Schematic illustrating production process of graphene nanoplatelets (GNPs) [Color figure can be viewed at wileyonlinelibrary.com]

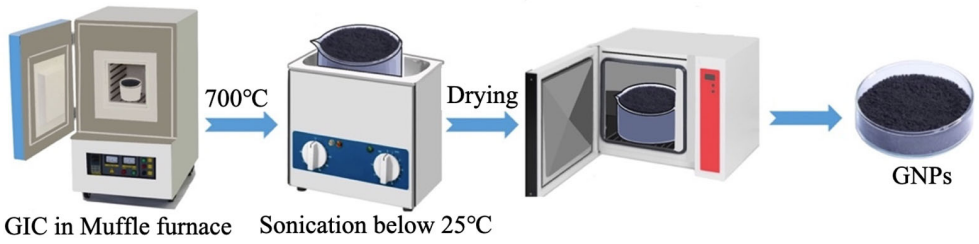

FIGURE 3 Schematic of process for coating a knitted fabric with graphene nanoplatelets (GNPs) [Color figure can be viewed at wileyonlinelibrary.com]

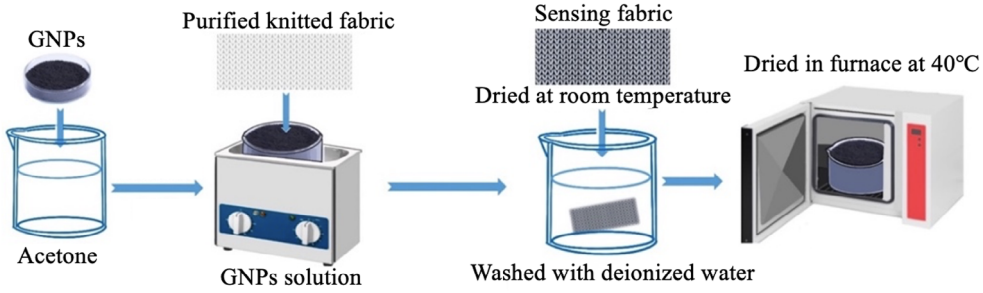

tension were chosen as the optimal settings for the selected yarns to reduce processing faults and to manufacture good quality knitted fabrics. All of the fabrics were designed with full needle knitting structures and were knitted to the same dimensions of 20 mm × 60 mm × 1.5 mm, with a height of 25 rows and width of 45 needles. The resulting fabrics can be seen in Figure 1.

2.2.2 | Fabrication of GNPs

GNPs were fabricated by a published method[47,48] as illustrated in Figure 2. In brief, graphite intercalation compounds are placed in a crucible and heated in a muffle furnace at 700°C for 2–3 min. The compounds thermally expanded into a worm-like structures after heating which are then placed in an acetone solution (below 25°C) using an ultrasonic bath for 3–4 h. The contents are then dried in an oven at 80°C overnight after sonication, creating GNPs.

2.2.3 | Fabrication of graphene/knitted fabrics

The sensing fabrics were fabricated by dip-coating the knitted fabrics with GNPs using an ultrasonication bath, as is shown in Figure 3. The prepared fabrics (cotton, merino wool, lambswool, silk and acrylic/Spandex) were first cleaned by soaking them in ethanol and then thoroughly washed with deionized water. After drying, the pre-cleaned fabrics were dipped into the prepared GNPs/acetone suspension with sonication for 30 min. Then the fabrics were rinsed with deionized water and dried in a furnace at 40°C.

This fabrication process was repeated with different GNP suspension proportions (0.3, 0.6, 0.9, 1.2, and 1.5 wt %) at different deposition times (10 min, 20 min, or 30 min of sonication). A total of 45 fabric samples were produced with 3 samples for each GNP fraction at each deposition time. The 3 fabric samples are then assigned to have either 1, 2, or 3 dipping cycles.

2.3 | Characterization

In the initial fabric selection test, the resistance changes and length of elongation of each sample were measured while being stretched from rest to its limit strain three times. The average resistance changes and length of elongation of each material with its respective SD were then calculated.

Images and thickness measurements of the GNPs were taken using an atomic force microscope (AFM, Dimension ICON2-SYS, Brook company, United States). A graphene nanosheet was randomly selected from GNPs solution and the average thickness was then calculated by measuring the thickness at 2 regions of the graphene nanosheet.

The surface of original knitted fabric and the cross-section of fabrics which fabricated with 0.3 and 1.2 wt% GNPs were also examined using a scanning electron microscope (SEM, SU8010, Hitachi, Japan) with an operating voltage of 5 kV to explore how changes in proportion of GNPs in solution affect the amount of deposited GNPs.

In the electrical property tests, the resting resistance of each knitted sensing fabric was measured three times using a Fluke data acquisition unit (2638A, Fluke, United States) and the weight of deposited GNPs in each fabric sample was measured using a laboratory scale to determine the optimal GNPs solution concentration and deposition time for the sensor fabrication process.

In mechanical property tests, the ultimate strain and limit tensile stress within the working range of sensing fabrics were measured using a universal tensile machine (GX-SF001, Shenzhen Shared Instrument Equipment Co. Ltd, China). The overall size of fabrics was 60 mm × 20 mm × 0.23 ± 0.03 mm and the tensile machine was set up to stretch fabrics at speed of 25 mm/min with gauge length of 5 cm, at room temperature (25°C).

The sensing properties of the graphene-coated sensing fabrics were evaluated by monitoring the change in resistance using a Fluke data acquisition unit while being stretched by a tensile machine at a speed of 25 mm/min. The sensitivity of sensing fabric is represented by the gauge factor (GF), which is the ratio of the relative changes in electrical resistance values (R) to the applied tensile strain. The GF of the sensing fabric was calculated using the following equation:

$$\mathrm{GF} = \frac{\Delta R/R}{\Delta L/L} \tag{1}$$

where R = initial resistance, $\triangle R$ = relative change in resistance under deformation, L = initial length of the sensor, and $\triangle L$ = change in length in the axial direction.

For the durability test, strain sensor was stretched and released by a tensile machine for 500 cycles with a strain rate of 30% at 0.25 Hz. The Fluke data acquisition unit was also applied to measure the change in resistance continually during each cycle.

Further response time test was conducted using again the tensile machine and the Fluke data acquisition unit. The knitted sensor was stretched at a constant speed from a static position with no strain to 30% strain over 15 s. The sensor was then released gradually back to its initial static position over 30 s. The time delay between change in resistance and change in strain was calculated three times (at 0, 15, and 30 s) to measure the response time.

In the sensor application section, the graphene-based textile sensor was attached to the extensor surfaces of four different joints including finger, wrist, elbow and knee, at a standard anatomically neutral or straight position (0°). The change in resistance was then measured using a Fluke data acquisition unit during repeated joint movements of each joint from 0° to 45° of flexion and 0°–90°of flexion, respectively. The change in resistance was then visually compared to the movement of the joint.

The electrochemical properties of knitted sensing fabrics were analyzed by testing cyclic voltammetry (CV), galvanostatic charge/discharge (GCD), cyclic stability measurement, and electrochemical impedance spectroscopy (EIS), using an electrochemical workstation (CHI660E B19038, Chenhua Instrument CO., Shanghai, China). A three-electrode supercapacitor device was set up, using 1 M Na_2SO_4 solution as the electrolyte and using a Pt sheet as counter electrode, Ag/AgCl sheet as reference electrode and our graphene-coated fabric as working electrode. The cyclic voltammetry (CV) curves were generated at a scan rate from 20 to 100 mV/s. The specific capacitance (C) was calculated from the area in the CV curve by the equation below:

$$C = \frac{\int IdV}{\upsilon \Delta V m} \tag{2}$$

Using the same three-electrode set up, the specific capacitance value at the current densities in GCD curves are calculated by equations below:

$$C = \frac{I \cdot \Delta t}{m \cdot \Delta \upsilon} \tag{3}$$

Where I = current (A), υ = scan rate ($V{\cdot}s^{-1}$), V = working potential, m = weight of graphene in the fabrics (g), and Δt = discharging time.

The cyclic stability test was conducted at a current density of 2 A/g, charging and discharging 10,000 times. The Nyquist curve was produced using data collected

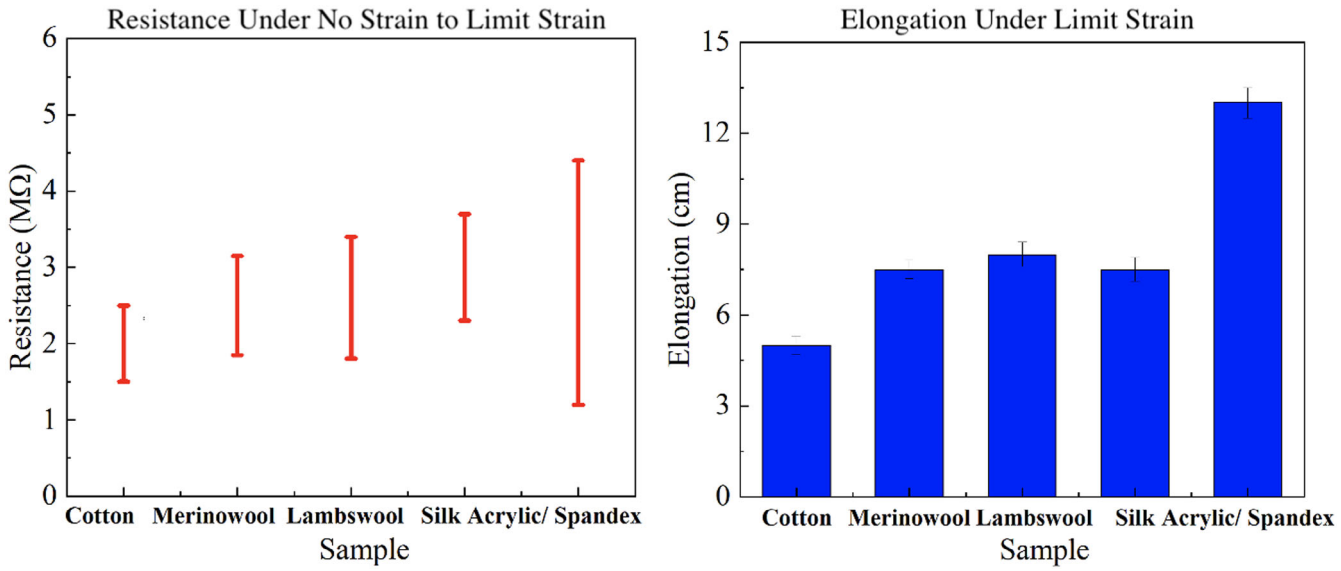

FIGURE 4 Change in resistance under no strain to the limit strain (left) and elongation of the fabric sensor the under limit strain (right) [Color figure can be viewed at wileyonlinelibrary.com]

through the EIS and the impedance was measured through a decreasing AC frequency.

For the cyclic sensing performance test of the capacitive sensor, the graphene-based fabric was mounted on the tensile testing machine for compression test. The graphene-based knitted fabric was compressed to 24.5 kPa and then released, repeated 10,000 cycles at 3.33 Hz, and the electrochemical workstation was used to measure the capacitance of the fabric.

3 | RESULTS AND DISCUSSION

3.1 | Fabric selection

Initial tests were performed to select the fabric with the most promising characteristics. That fabric was then analyzed in further tests outlined in the following sections. It can be seen from Figure 4 (left) that the acrylic/Spandex fabric has the largest resistance range out of all the fabrics, making it suitable for detecting various degrees of movement. As shown in Figure 4 (right), acrylic/Spandex fabrics has much larger sensing range due to its ability to stretch much further than the other types of fabrics. Therefore, the acrylic/Spandex fabrics were selected for fabrication characterization, presented in the following tests.

3.2 | Morphology of GNPs

As shown in Figure 5, one graphene nanosheet was used to investigate its micromorphology. The average thickness of the graphene nanosheet was measured at 3.48 ± 0.3 nm in alignment with thickness of.[48] Our 3 nm-thick graphene nanosheet has desirable specific surface area, which may provide sufficient interface area between the GNPs and the textile, and improve the mechanical and electrical performance of the fabrics.[49]

3.3 | Morphology of graphene-coated knitted fabrics

The SEM was used to examine the morphology of the knitted fabrics which fabricated at various fractions of GNPs. Figure 6a1–a3 show the microstructure of the original knitted fabrics surface. Figure 6a1 is an overview of the knitted fabrics, showing a uniform entwining structure of acrylic fibers. Figure 6a2 and a3 demonstrate magnified images of Figure 6a1. In Figure 6a2, knitted fabric shows relatively organized fiber structure to form a porous network. Furthermore, typical smooth and featureless acrylic fiber surface structures were observed in Figure 6a3.

Figure 6b1–b3 shows the cross-section of graphene-coated fabrics which prepared with a fraction of GNPs at 0.3 wt%. As shown in Figure 6b1, there is only small amount of graphene dispersed randomly on the surface of the fibers. At a higher magnified Figure 6b2, GNPs can be found in the fiber gaps.

Figure 6c1–c3 are SEM images of the graphene-coated fabrics which fabricated at a fraction of GNPs at 1.2 wt%. It can be seen that the overall amount of GNPs have significantly increased in Figure 6c1 compared to

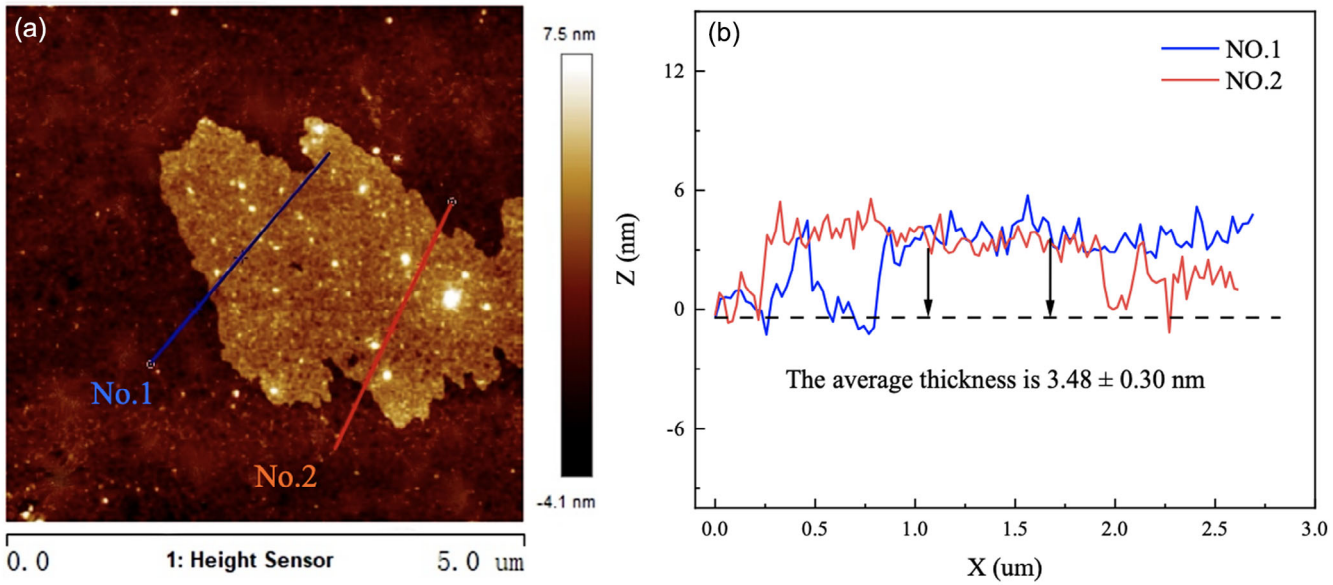

FIGURE 5 (a) Atomic force microscope (AFM) micrographs and (b) thickness measurement of graphene nanoplatelets (GNPs) [Color figure can be viewed at wileyonlinelibrary.com]

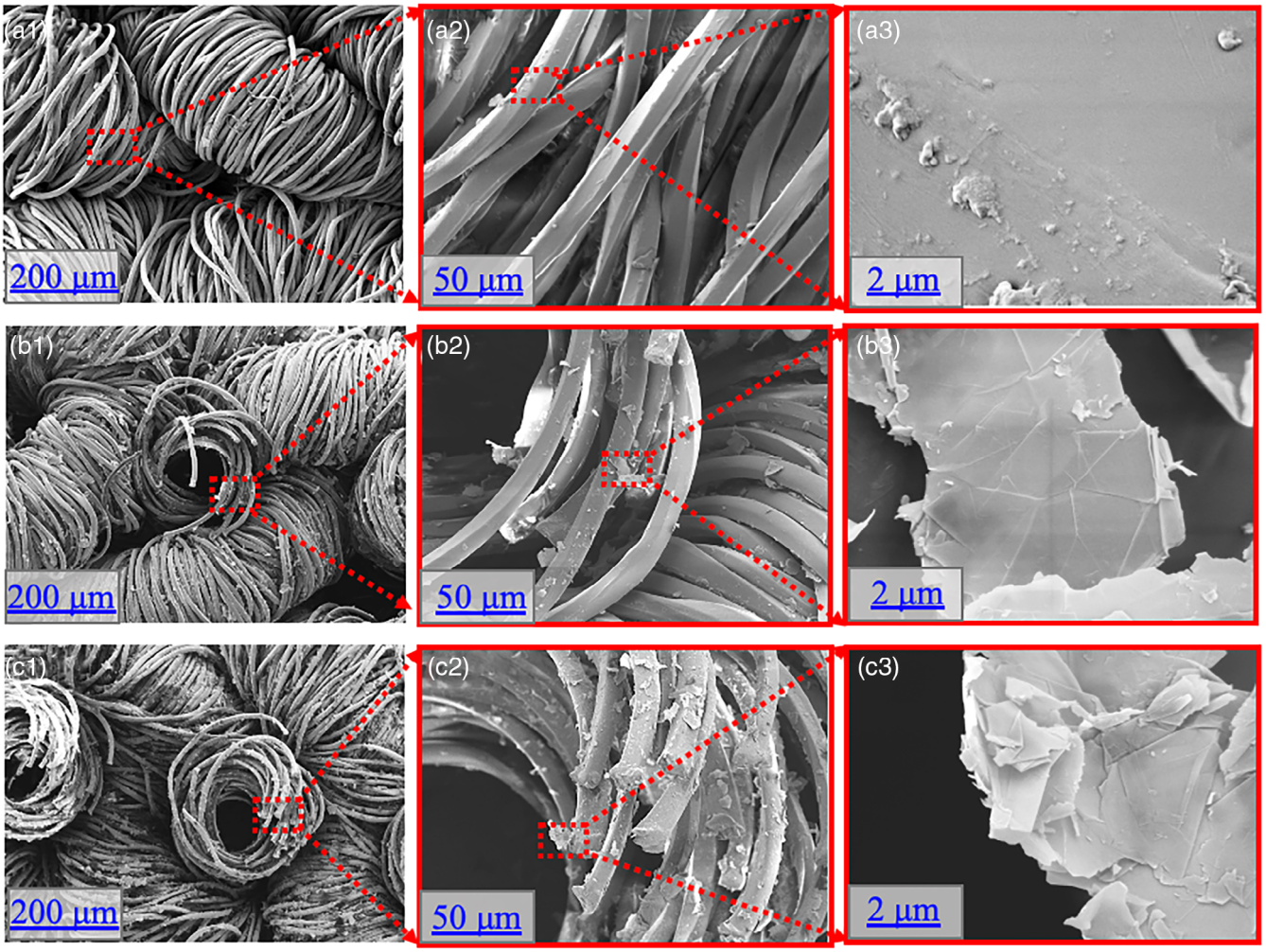

FIGURE 6 Scanning electron microscope (SEM) images of surface of the original knitted fabrics (a1-a3), and the cross-section of the fabrics fabricated with 0.3 wt% graphene (b1-b3) and 1.2 wt% graphene (c1-c3) [Color figure can be viewed at wileyonlinelibrary.com]

Figure 6b1. It can be seen from Figure 6c2 that the GNPs have attached evenly to the surface of textile fibers, indicating GNPs have been successfully assembled on the fabric. The typical structures of GNPs on the acrylic fibers are further magnified and demonstrated in Figure 6b3 and c3, which exhibit a typical wrinkled structure.

Overall, the porous fiber network shown in Figure 6a1–c1 is able to build up conductive composite structure (GNPs in Figure 6b,c). With the high specific surface area of the fiber matrix along with highly conductive graphene, this demonstrates our sensor also has great potential in capacitive applications.[45]

3.4 | Electrical properties

The electrical property of graphene-coated fabrics is closely related to its fabrication process,[50] so it is crucial to examine the effects of differing GNPs proportions in the suspension, the deposition time, and the number of dip coating cycles on the electrical conductivity of the graphene-coated fabrics during the fabrication process. Figure 7a illustrates the electrical property of the graphene-coated fabrics as a function of GNPs concentration. As the fraction of GNPs increases from 0.3 to 1.5 wt%, the resistance of sensing fabrics decreases rapidly and eventually flattening out when the concentration reached 1.2 wt%. This is likely due to the sensing fabrics becoming fully saturated with GNPs.

To verify whether the 1.2 wt% GNPs is the saturation point for the deposition of fabrics, the amount of graphene deposited in the fabrics was measured using a laboratory scale, which is shown in Figure 7b. The GNPs adsorption increases linearly and finally measuring at 15 mg, when the GNPs concentration increases to 1.5 wt %, which is similar to 1.2 wt%. Therefore, 1.2 wt% was found to be the saturation point and is set to be the control in the following tests on the effect of deposition time and dip counts on electrical conductivity.

In Figure 7c, as the deposition time increases, the resting resistance of the sensing fabric sharply decreases, reaching 48 kΩ after 30 min of deposition. Then, we tested different times for the dip-coating cycles with the same 30-min deposition time, as shown in Figure 7d. The resistance of the sensing fabrics decreases exponentially and flattens out to 8 kΩ as the number of dip-coating

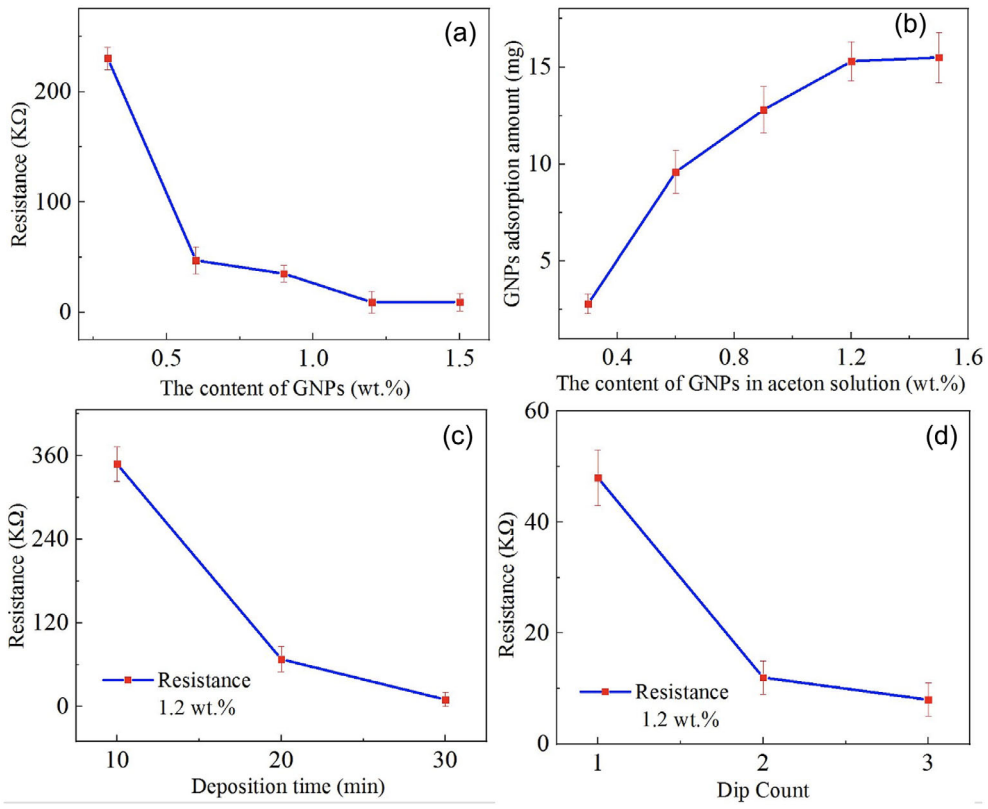

FIGURE 7 (a) Resistance of graphene coated fabrics against different proportions of graphene nanoplatelets (GNPs); (b) deposited amount of GNPs on the fabrics against various proportions of GNPs in the suspension; (c) resistance of the graphene-coated fabrics against deposition time; (d) resistance of the graphene-coated fabrics against number of dip-coating cycles [Color figure can be viewed at wileyonlinelibrary.com]

cycles increase from one to three. Therefore, we decided to produce sensing fabrics with 1.2 wt% GNPs, 30-min deposition time and 3 dip-coatings to further explore their sensing properties.

3.5 | Mechanical properties

Tensile strength and elongation at break are crucial for characterizing the mechanical properties of a material. However, the graphene-coated fabric samples are composed of textile fabrics with compact structures and increased elasticity, leading them to be difficult to break. Therefore, we tested the ultimate stress and limit strain within the sensing range of the sensing fabrics to observe the effect of GNPs fraction to mechanical performance of the graphene-coated fabrics.

Figure 8 shows the ultimate stress and limit strain of fabrics produced in different fractions of GNPs. As shown in Figure 8a, the ultimate stress increases linearly with the increase of GNPs concentration, and level out once fraction of GNPs reached to 1.2 wt%. The maximum ultimate stress is calculated to be 0.18 Mpa at 1.5 wt% of GNPs. The increase in ultimate stress is due to the increased adsorption of GNPs, which produces more rigid chemical structures and requires a larger stress to stretch the fabrics.

Figure 8b demonstrates a similar linear shape to Figure 8a, as the GNPs fraction increases, the limit strain of graphene coated fabrics increases rapidly reaching 348% at 1.5 wt% of GNPs. This is because the increase in graphene concentration enhances the electrical conductivity and broadens the sensing range of the graphene-coated fabrics.

Figure 8c shows typical stress–strain curves during stretching of fabrics with different concentration of GNPs, which demonstrates that more tensile stress is required to achieve the same strain as the concentration of GNPs increases. In conclusion, the increase in GNPs fraction improves the mechanical properties of the knitted fabrics.

3.6 | Sensing properties

The sensing property test of our graphene-coated knitted sensor consisted of sensitivity, durability, and response time tests. In a high-performance strain sensor, the change in resistance should have a linear relationship with the tensile strain to obtain accurate electrical signals.[14,51]

Figure 9a demonstrates the sensing mechanism of graphene-coated sensing fabrics. When the sensing fabric was stretched, the GNPs deposited on the fabric also deforms along with the knitted structure, which increases the inter-distance between GNPs, resulting in increased electrical resistance. The overall conductivity of the sensor is not necessarily directly related to the performance of the sensor. When the range of the resistance change is greater, the sensor is more sensitive, and making it more ideal for human motion monitoring of small movements. In Figure 9b, the resistance change rate of knitted sensor increases uniformly with increase in strain. The sensing fabric exhibits two linear regions with high GFs of 3 and 16 under the extremely large strains of 0%–175% and 175%–344%, indicating that our sensor has excellent stretchability and sensitivity.

Figure 9c reflects the strain sensor being stretched incrementally for 10 mm and held in place for 15 s until reaching 50 mm. The relative change in resistance of the sensor increases significantly to a certain value, then decreases slightly and remains stable during the measurement time of 15 s for each stretch. This is due to the relaxation phenomenon caused by viscoelasticity of the

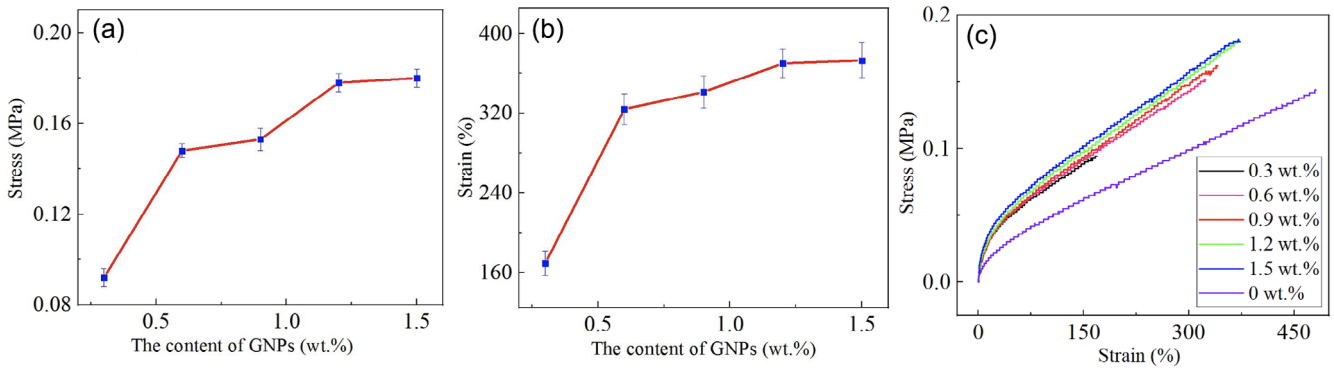

FIGURE 8 (a) Ultimate stress of graphene coated fabrics against fractions of graphene nanoplatelets (GNPs); (b) limit strain of graphene coated fabrics against proportions of GNPs; (c) tensile test of fabrics with different proportions of GNPs [Color figure can be viewed at wileyonlinelibrary.com]

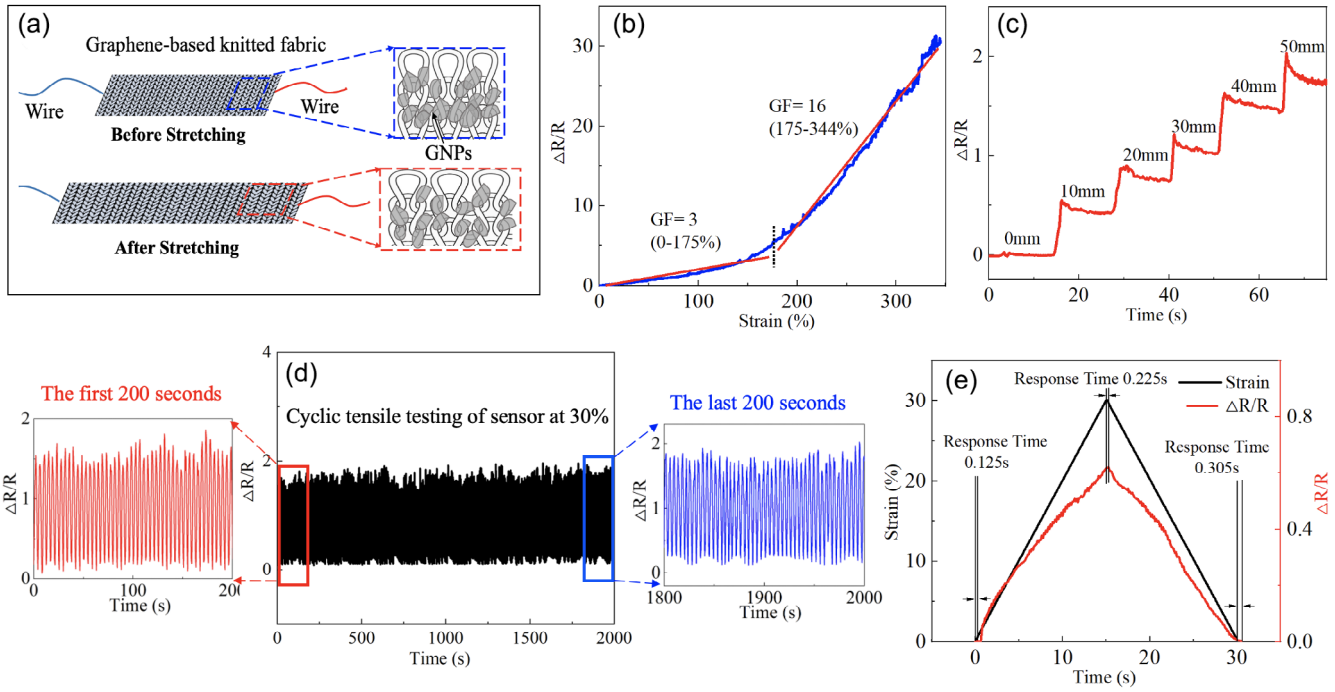

FIGURE 9 (a) Schematic of sensing mechanism; (b) strain against change in resistance of knitted strain sensor; (c) relative change in resistance against time held at stretching distance of 0 mm, 10 mm, 20 mm, 30 mm, 40 mm and 50 mm; (d) durability test of strain sensor under 30% strain over 500 cycles; (e) response time test under tension and release of 30% strain [Color figure can be viewed at wileyonlinelibrary.com]

fabrics which when the strain value suddenly increases, all parts of the sensor will deform under this strain. However, after a period of time, the resistance decreases with the relaxation of the fabric.[32]

As shown in Figure 9d, cyclic tensile test was conducted to examine the stability and durability of the strain sensor. The strain sensor was stretched and released at 30% strain for 500 cycles at a frequency of 0.25 Hz. During the first 200 s, the magnitude of resistance change rate of the sensor experiences some fluctuations and then gradually stabilizes. This is due to the internal structures of the knit fabric adapting to the applied force in the early stage of the cyclic test.[23] After 500 cycles, strain sensor showed significant durability, stability, and reproducibility, maintaining similar change in resistance.

Response time is an important characteristic to examine response ability of sensors to strain,[19] and a test for response time of the sensors was conducted (Figure 9e). The graphene sensor was put in a static position with 0% strain at 0 s and was stretched at a constant speed to reach 30% strain at 15 s. Then, the sensor was released gradually back to its initial position at 30 s. The response time was then measured three times, comparing the time delay between $\triangle R$ and the change in strain at 0 and 15 s, also the time delay for $\triangle R$ to return to 0 when strain reached 0 at 30 s. Figure 9e demonstrates that our sensor experienced a degree of elastic hysteresis corresponding to its resistance change, with the average response time being about 0.2 s.

The sensing performance of our sensor and other reported sensors were further compared, as shown in Table 1. Overall, our graphene-coated sensor shows desirable sensitivity and stretchability, comparing to some similar graphene-based textile strain sensors.

3.7 | Sensor applications

Graphene-based textile sensors are flexible, highly sensitive and lightweight, so it can be implemented as wearables and have a huge potential for body motion monitoring. In this exploratory study, four typical body movements were studied, including areas with smaller movements such as fingers and wrist joints, and areas with a larger range of motion such as the elbows and knee joints.

It can be seen in Figure 10 that the change in resistance for all four types of body joints shows a very similar trend. When body joints are at their initial position at 0°, the change in resistance remains at ~0. With each joint movement, the change in resistance increases to a certain level and then drops back to 0 almost instantly when the

TABLE 1 Comparison between reported textile strain sensor and our sensor

Type	Stretchable component	Sensing component	Sensing range (%)	Gauge factor	Linearity	Reference
Silicone fiber	PDMS	Ionic liquid	100	0.5	Two linear regions	43
Nylon filament	Nylon	GNPs	46	0.94	Three linear regions	41
Flax yarn	Ecoflex	GNPs/CBs	50	0.1	Two linear regions	42
Nylon strip	Nylon	$Ti_3C_2T_x$ nanosheets	50	2.4	NA	52
Wool yarn	Ecoflex	GNPs/CBs	200	7.75	Two linear regions	53
Wool woven fabric	PDMS	GNPs	3	223	One linear region	44
Cotton knitted fabric	cotton	AuNWs	150	0.31	Two linear regions	45
Acrylic/Spandex knitted fabric	Spandex	GNPs	344	16	Two linear regions	This work

Abbreviation: GNPs, graphene nanoplatelets.

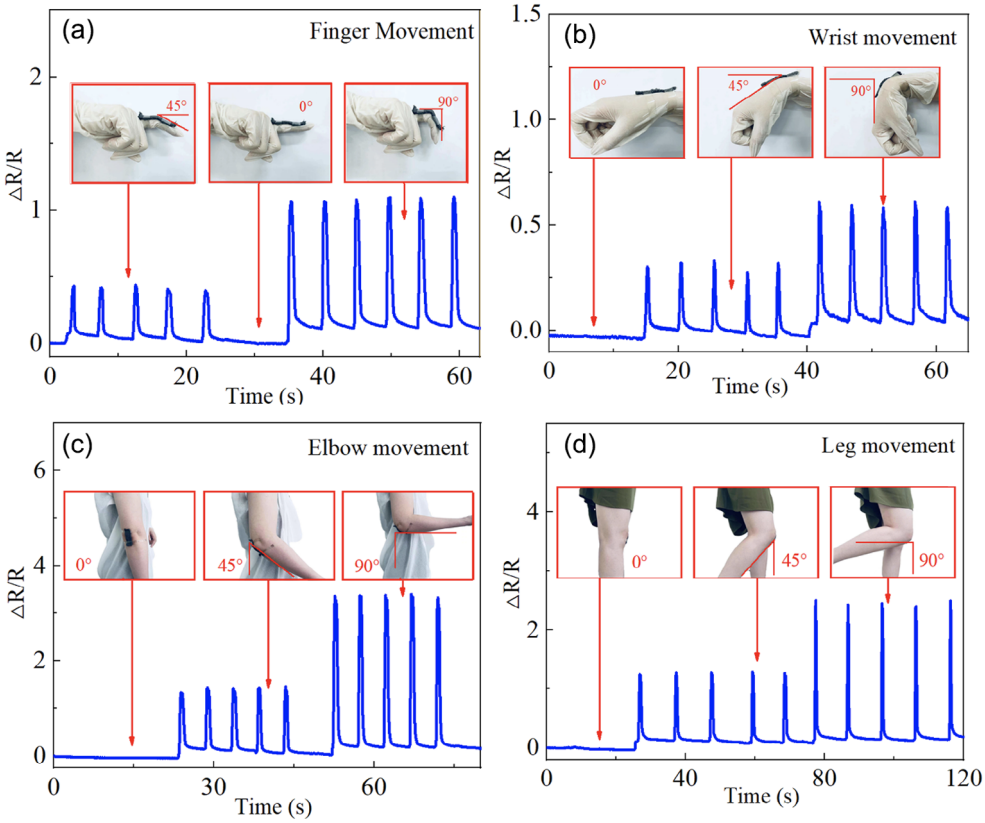

FIGURE 10 Experiment images and corresponding time-instant response curves of the sensing system as the human motion monitoring: (a) finger, (b) wrist, (c) elbow joint, and (d) knee joint [Color figure can be viewed at wileyonlinelibrary.com]

joint returns to its resting positing. This indicates that our sensors are reliable in distinguishing each separate joint movement. As the range of movement increases from 45° to 90°, the peak $\triangle R$ for each movement also increases by approximately twofold for all joints. This shows that our sensors are capable to differentiate between various ranges of joint movements. The peak $\triangle R$ also remains very similar with each successive joint movement at 45° and 90° which indicates high precision for our sensors in measuring repeated movements.

Together with its advantages of being light weight, low cost, and easy integration with everyday clothing, our sensor has great potential to be used as an objective daily monitoring tool for posture and gait, also possibly detecting abnormal movements or movement impairment in certain neurological disorders. Further in-depth study of the performance of the sensor on the body using a secondary motion-tracking system is needed to draw more rigorous conclusions, but the initial performance is promising.

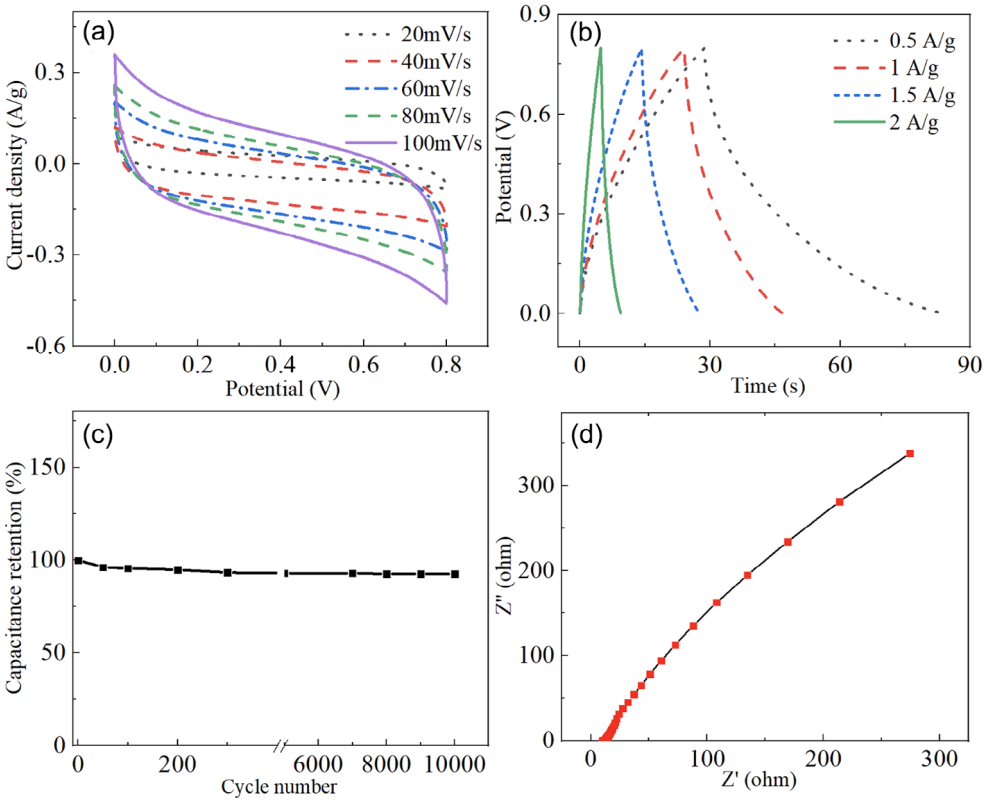

FIGURE 11 (a) Cyclic voltammetry (CV) curves of fabrics prepared with 1.2 wt% graphene at different scanning rates; (b) galvanostatic charge/discharge (GCD) curves of graphene-coated knitted fabrics; (c) cyclic stability of graphene-coated knitted fabrics; (d) Nyquist diagram of graphene-coated knitted fabrics [Color figure can be viewed at wileyonlinelibrary.com]

3.8 | Electrochemical performance and capacitive pressure sensor

The knitted fabrics used in this experiment are weft-knitted fabrics, which made with two sets of needle beds. The porous structure of the fabrics enhances the specific surface area and facilitates the formation of a conductive network, resulting in the improvement of electron and ion transport kinetics, sharing similar properties between a supercapacitor or a capacitive pressure sensor. The electrochemical properties of graphene knitted fabrics applied as a capacitor were studied by testing CV and constant current charge and GCD measurements, which are shown in Figure 11.

Figure 11a demonstrates the CV curve of 1.2 wt% graphene-coated fabrics. When the scan rate is increases from 20 to 100 mV/s, the corresponding specific capacitance decreases from 32 to 13.6 F/g. It can be seen that all CV curves show a similar shape at different scanning speeds, indicating our knitted fabrics have good capacitance performance.

Graphene-coated fabrics were then applied to conduct GCD test at the current density of 0.5, 1, 1.5, and 2 A/g. As shown in Figure 11b, the specific capacitance value decreases with the increase in current density which the capacitance values of 31.7, 26.5, 18.2, and 11.5 F/g were measured at current densities of 0.5, 1, 1.5, and 2 A/g respectively. The 1.2 wt% graphene-coated fabrics exhibit a linear and symmetrical GCD curve, which demonstrates that our knitted fabric has good electrochemical performance.

The cyclic stability of the graphene-coated knitted fabric was examined. As shown in Figure 11c, the capacitance retention of our graphene-coated fabric remains above 90% after 10,000 charging and discharging cycles, reflecting its reliable cyclic stability. This is due to the stable textile structure of our graphene-coated fabrics, and the GNPs attached to the inner structure of textile can act as a good electron shuttle, resulting in more stable capacity retention.

Figure 11d reflects the Nyquist plot of graphene-coated fabrics. The Nyquist curve was produced using data collected through EIS which measures impedance with a decreasing AC frequency. The almost imperceptible semicircle plot reveals an extremely low charge transfer resistance for graphene-coated fabrics and the ion diffusion resistance of the graphene-coated fabrics was calculated to be 20 Ω.

Figure 12 demonstrates the possibility of applying graphene coated fabrics as a capacitive pressure sensor. As shown in Figure 12a, the rate of change in capacitance increases with incremental changes in pressure. The capacitance rate of knitted fabrics presents two linear regions, first increasing to 22% during pressure range of 0–9.8 kPa and further increasing at a slower rate to 43% from 9.8 to 24.5 kPa. Figure 12b shows the response time

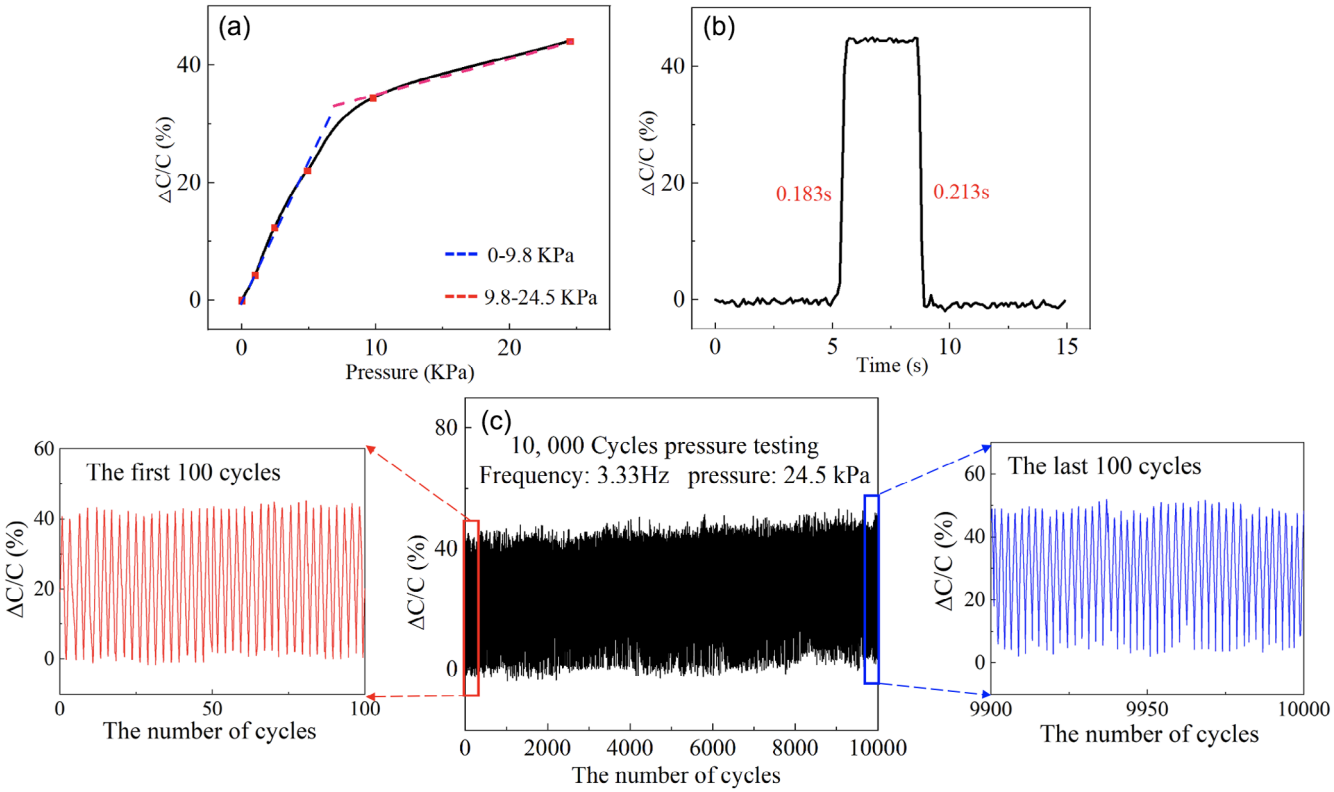

FIGURE 12 (a) Rate of change in capacitance as pressure applied within 0–24.5 kPa; (b) response and recovery time test under loading and unloading pressure; (c) durability testing under 24.5 kPa [Color figure can be viewed at wileyonlinelibrary.com]

and the recovery time of graphene coated fabrics under the loading and unloading pressure of 24.5 kPa. The knitted fabrics exhibits fast response and recovery times of 0.183 and 0.213 s respectively, indicating great sensitivity and stability.

The durability test was also performed to examine the cyclic sensing performance of the capacitive sensor. As shown in Figure 12c, the change in capacitance rate demonstrated good repeatability and stability in the long compressing cycles except for a slight shift, and the deviation between the changes in capacitance before and after 10,000 cycles was calculated as 13.9%, indicating that our graphene-based knitted fabric exhibits long–term durability when worked as a capacitive pressure sensor.

4 | CONCLUSION

By using a simple dip-coating method and ultrasonication bath, we reliably designed and developed a highly stretchable and flexible graphene-based textile strain sensor. After comparing five different yarns using a double bed knitting machine to produce the fabric samples, the strain sensor was fabricated with acrylic/Spandex yarn. It has outstanding stretchability and exhibited a high GF up to 16 under a limit strain of 344%, which is higher than the other similar graphene-based sensors. Our sensor is able to detect both large and subtle human movements and to differentiate various ranges of joint movements, making it suitable for integration into wearables. As such it has significant potential in human motion monitoring. Furthermore, our sensor expressed the ability to build up and discharge electrical charges, which showed its capability to be applied as a supercapacitor or capacitive type pressure sensor.

Future research into graphene-based textile sensors should focus on the requirements and limitations of the application of such sensors on human skin for a long period of time and outdoor ambulatory applications. The integration method, washability, reliability and longevity of sensors need to also be evaluated when fully incorporated into a device or product.

AUTHOR CONTRIBUTIONS

Yi Zhou: Conceptualization (lead); data curation (lead); formal analysis (lead); investigation (lead); methodology (lead); writing – original draft (lead). **Connor Myant:** Supervision (lead). **Rebecca Stewart:** Supervision (lead); writing – review and editing (lead).

ACKNOWLEDGMENTS

The authors would like to thank Yin Yu for her advice during the research.

DATA AVAILABILITY STATEMENT

Research data are not shared.

ORCID

Yi Zhou https://orcid.org/0000-0002-4176-5793

REFERENCES

[1] Z. Guo, M. Liu, Z. Cong, W. Guo, P. Zhang, W. Hu, X. Pu, *Adv. Mater. Technol.* **2020**, *5*, 2000544.
[2] A. Levitt, J. Zhang, G. Dion, Y. Gogotsi, J. Razal, *Adv. Funct. Mater.* **2020**, *30*, 2000739.
[3] T. Nguyen, J. Park, *J. Appl. Polym. Sci.* **2011**, *121*, 3596.
[4] C. Zhu, R. Li, X. Chen, E. Chalmers, X. Liu, Y. Wang, B. Xu, X. Liu, *Adv. Sci.* **2020**, *7*, 2002009.
[5] X. Pu, S. An, Q. Tang, H. Guo, C. Hu, *iScience* **2021**, *24*, 102027.
[6] E. Li, X. Lin, B. Seet, F. Joseph, J. Neville, in *IEEE Int. Instrum. Measur. Technol. Conf. (I2MTC)* **2019**, pp. 1–5.
[7] K. Arquilla, A. Webb, A. Anderson, *Sensors* **2020**, *20*, 1013.
[8] S. Afroj, S. Tan, A. Abdelkader, K. Novoselov, N. Karim, *Adv. Funct. Mater.* **2020**, *30*, 2000293.
[9] Y. Huang, L. Gao, Y. Zhao, X. Guo, C. Liu, P. Liu, *J. Appl. Polym. Sci.* **2017**, *134*, 45340.
[10] A. Hatamie, S. Angizi, S. Kumar, C. Pandey, A. Simchi, M. Willander, B. Malhotra, *J. Electrochem. Soc.* **2020**, *167*, 037546.
[11] Z. Lou, L. Wang, K. Jiang, Z. Wei, G. Shen, *Mater. Sci. Eng. R: Rep.* **2020**, *140*, 100523.
[12] S. Afroj, N. Karim, Z. Wang, S. Tan, P. He, M. Holwill, D. Ghazaryan, A. Fernando, K. Novoselov, *ACS Nano* **2019**, *13*, 3847.
[13] K. Chang, M. Li, W. Zhong, Y. Wu, M. Luo, Y. Chen, Q. Liu, K. Liu, Y. Wang, Z. Lu, D. Wang, *J. Appl. Polym. Sci.* **2019**, *136*, 47928.
[14] A. Liang, R. Stewart, N. Bryan-Kinns, *Sensors* **2019**, *19*, 3618.
[15] J. Park, W. Hyun, S. Mun, Y. Park, O. Park, *ACS Appl. Mater. Interfaces* **2015**, *7*, 6317.
[16] X. Xiang, H. Li, Y. Zhu, S. Xia, Q. He, *J. Appl. Polym. Sci.* **2021**, *138*, 50801.
[17] D. Zhang, R. Yin, Y. Zheng, Q. Li, H. Liu, C. Liu, C. Shen, *Chem. Eng. J.* **2022**, *438*, 135587.
[18] H. Lee, M. Glasper, X. Li, J. Nychka, J. Batcheller, H. Chung, Y. Chen, *J. Mater. Sci.* **2018**, *53*, 9026.
[19] Y. Bu, T. Shen, W. Yang, S. Yang, Y. Zhao, H. Liu, Y. Zheng, C. Liu, C. Shen, *Sci. Bull.* **2021**, *66*, 1849.
[20] Y. Zhou, C. Zhang, C. Myant, R. Stewart, Knitted Graphene Supercapacitor and Pressure-Sensing Fabric, *E-Textiles 2021* **2022**.
[21] G. Islam, A. Ali, S. Collie, *Cellulose* **2020**, *27*, 6103.
[22] L. Possanzini, M. Tessarolo, L. Mazzocchetti, E. Campari, B. Fraboni, *Sensors* **2019**, *19*, 4686.
[23] O. Atalay, W. Kennon, M. Husain, *Sensors* **2013**, *13*, 11114.
[24] Y. Zheng, R. Yin, Y. Zhao, H. Liu, D. Zhang, X. Shi, B. Zhang, C. Liu, C. Shen, *Chem. Eng. J.* **2021**, *420*, 127720.
[25] Z. Zhou, N. Chen, H. Zhong, W. Zhang, Y. Zhang, X. Yin, B. He, *Materials* **2021**, *14*, 6073.
[26] H. Souri, D. Bhattacharyya, *ACS Appl. Mater. Interfaces* **2018**, *10*, 20845.
[27] H. Liu, Q. Li, Y. Bu, N. Zhang, C. Wang, C. Pan, L. Mi, Z. Guo, C. Liu, C. Shen, *Nano Energy* **2019**, *66*, 104143.
[28] S. Seyedin, J. Razal, P. Innis, A. Jeiranikhameneh, S. Beirne, G. Wallace, *ACS Appl. Mater. Interfaces* **2015**, *7*, 21150.
[29] Z. Yang, Y. Pang, X. Han, Y. Yang, J. Ling, M. Jian, Y. Zhang, Y. Yang, T. Ren, *ACS Nano* **2018**, *12*, 9134.
[30] C. de Oliveira, M. Batistella, S. de Souza, A. de Souza, *J. Appl. Polym. Sci.* **2017**, *134*, 44785.
[31] I. Krucińska, B. Surma, M. Chrzanowski, E. Skrzetuska, M. Puchalski, *J. Appl. Polym. Sci.* **2012**, *127*, 869.
[32] K. R. Reddy, S. Gandla, D. Gupta, *Adv. Mater. Interfaces* **2019**, *6*, 1900409.
[33] A. Tarhini, A. Tehrani-Bagha, M. Kazan, B. Grady, *J. Appl. Polym. Sci.* **2020**, *138*, 49821.
[34] Y. Zheng, H. Xu, H. Jing, Q. Ren, Z. Liu, Z. Gao, Q. Ban, *J. Appl. Polym. Sci.* **2022**, *139*, 52110.
[35] H. Ye, H. Jiang, Z. Luo, L. Xu, *J. Appl. Polym. Sci.* **2021**, *139*, 52030.
[36] N. Celik, N. Manivannan, A. Strudwick, W. Balachandran, *Nanomaterials* **2016**, *6*, 156.
[37] J. Ren, C. Wang, X. Zhang, T. Carey, K. Chen, Y. Yin, F. Torrisi, *Carbon* **2017**, *111*, 622.
[38] N. Karim, S. Afroj, S. Tan, P. He, A. Fernando, C. Carr, K. Novoselov, *ACS Nano* **2017**, *11*, 12266.
[39] F. Banhart, J. Kotakoski, A. Krasheninnikov, *ACS Nano* **2010**, *5*, 26.
[40] J. Potts, D. Dreyer, C. Bielawski, R. Ruoff, *Polymer* **2011**, *52*, 5.
[41] M. Tian, R. Zhao, L. Qu, Z. Chen, S. Chen, S. Zhu, W. Song, X. Zhang, Y. Sun, R. Fu, *Macromol. Mater. Eng.* **2019**, *304*, 1900244.
[42] H. Souri, D. Bhattacharyya, *Mater. Des.* **2018**, *154*, 217.
[43] S. Chen, H. Liu, S. Liu, P. Wang, S. Zeng, L. Sun, L. Liu, *ACS Appl. Mater. Interfaces* **2018**, *10*, 4305.
[44] X. Liu, C. Tang, X. Du, S. Xiong, S. Xi, Y. Liu, X. Shen, Q. Zheng, Z. Wang, Y. Wu, A. Horner, J. Kim, *Mater. Horiz.* **2017**, *4*, 477.
[45] Z. Zhao, Q. Li, Y. Dong, J. Gong, Z. Li, X. Qiao, J. Zhang, *Energy Technol.* **2021**, *9*, 2100166.
[46] R. Yu, C. Zhu, J. Wan, Y. Li, X. Hong, *Polymer* **2021**, *13*, 151.
[47] S. Han, Q. Meng, K. Xing, S. Araby, Y. Yu, A. Mouritz, J. Ma, *Compos. Sci. Technol.* **2020**, *198*, 108312.
[48] Q. Meng, Y. Yu, J. Tian, Z. Yang, S. Guo, R. Cai, S. Han, T. Liu, J. Ma, *Nanotechnology* **2020**, *31*, 465502.
[49] S. Han, P. Wang, Y. Zhou, Q. Meng, M. Aakyiir, J. Ma, *Compos. Sci. Technol.* **2022**, 109451. Epub ahead of print.
[50] G. Cai, M. Yang, Z. Xu, J. Liu, B. Tang, X. Wang, *Chem. Eng. J.* **2017**, *325*, 396.
[51] L. Wang, K. J. Loh, *Smart Mater. Struct.* **2017**, *26*, 055018.
[52] K. Yang, H. Cheng, B. Wang, Y. Tan, T. Ye, Y. Yang, C. Wang, *Adv. Mater. Technol.* **2022**, *7*, 2100675.
[53] H. Souri, D. Bhattacharyya, *Sens. Actuators, A* **2019**, *285*, 142.

How to cite this article: Y. Zhou, C. Myant, R. Stewart, *J. Appl. Polym. Sci.* **2022**, e52755. https://doi.org/10.1002/app.52755